Maximizing Achievable Data Rate in Unlicensed mmWave Networks with Mobile Clients

Maximizing achievable data rate in unlicensed mmWave networks with mobile clients

Nadezhda Chukhno[1], Olga Chukhno[1], Sergey Shorgin[3], Konstantin Samouylov[1,3], Olga Galinina[2], and Yuliya Gaidamaka[1,3]

[1] Peoples' Friendship University of Russia, Russia
{nvchukhno,olgachukhno95}@gmail.com, {gaydamaka-yuv,samuylov-ke}@rudn.ru
[2] Tampere University, Finland
olga.galinina@tuni.fi
[3] Federal Research Center "Computer Science and Control" of the Russian Academy of Sciences, Russia
sshorgin@ipiran.ru

Abstract. In millimeter-wave (mmWave) networks, where faster signal attenuation is compensated by the use of highly directional antennas, the effects of high mobility may seriously harm the link quality and, hence, the overall system performance. In this paper, we study the channel access in unlicensed mmWave networks with mobile clients, with particular emphasis on initial beamforming training and beam refinement protocol as per IEEE 802.11ad/ay standard. We explicitly model beamforming procedures and corresponding overhead for directional mmWave antennas and provide a method for maximizing the average data rate over the variable length of the 802.11ad/ay beacon interval in different mobility scenarios. We illustrate the impact of the client speed and mobility patterns by examples of three variations of the discrete random walk mobility model.

Keywords: mmWave · beamforming · 802.11ad/ay · channel access · mobility · random walk .

1 Introduction

Millimeter-wave (mmWave) has become one of the most discussed wireless technologies of today, being recently included in the top ten trends that will drive innovation [1]. Even thought mmWave research has a long history, only recent advances in microelectronics and, more importantly, the rapidly growing popularity of bandwidth-hungry applications, such as virtual, augmented, and mixed reality (AR/VR/MR) have brought the technology closer to the mass adoption.

A promising mmWave carrier candidate to meet the growing consumer data demand can be found in the 60 GHz band, which is identified by FCC as a part of the unlicensed spectrum. At 60 GHz, two pioneering standards, Wireless HD and ECMA-387, published in 2008, and the first IEEE standard, the IEEE 802.15.3c-2009, approved in 2009, promised to provide real gigabit throughputs but did not become widely accepted due to a number of technical issues.

The first 60 GHz protocol in IEEE 802.11 family (Wi-Fi), 802.11ad, published in 2012, has already brought many commercial hardware products to the market. Its backward-compatible successor, the IEEE 802.11ay standard [2], has passed the Draft 3.1 stage and currently is approaching its final IEEE ratification, which is expected in March 2020[4]. The target use cases studied by the IEEE 802.11 TGay Group [3] include, among others, AR/VR headsets and other high-end wearables, where the access point and client devices could be highly mobile.

In the case of IEEE 802.11ad/ay protocols, where faster mmWave signal attenuation is compensated by the use of highly directional antennas, the effects of high mobility may seriously harm the link quality and the overall system performance. Fortunately, the respective IEEE specifications leave many protocol parameters flexible and implementation-dependent to be later tuned depending on the degree of mobility, as concrete use cases would require.

As the IEEE 802.11ad specification has been openly accessible since 2012, multiple research papers address evaluation, optimization, and other various aspects of the 802.11ad protocol [4–7], including a comparison of in-field experiments and simulation-based studies [8]. The latest 802.11ay, although not yet publicly available, has been described in detail in seminal papers [2, 9, 10] by Intel (one of the IEEE 802.11ay contributors), where [9] focuses on the beam refinement protocol (BRP) and asymmetric beamforming training, and [10] addresses fundamental elements of the single-carrier PHY of IEEE 802.11ay (the new frame format, modulation and coding schemes (MCSs), new beamforming training field, etc.).

Despite the surge of interest to IEEE 802.11ad/ay, the effect of mobility has received limited attention of the research community. For vehicular applications of 802.11ad, there have been proposed several learning-based sweeping solutions, including non-supervised online learning algorithms for beam pair selection and refinement [11], sparsity-aware beamforming design for radars [12], and multipath fingerprinting algorithm for the beam alignment [13]. The effects of mobility in mmWave have also been addressed in [14, 15] in the context of blockers mobility, however, without any protocol linked.

In this paper, we study the channel access of IEEE 802.11ad/ay, with particular emphasis on initial beamforming training and beam refinement protocol. We explicitly model beamforming procedures and corresponding overhead for highly directional antennas and maximize the average data rate over the variable length of the 802.11ad/ay beacon interval. Our main contribution lies in providing a method for maximizing the average data rate in various mobility scenarios. The impact of the client speed and mobility patterns is illustrated by selected numerical results when using examples of three diverse variations of the discrete random walk mobility model.

The rest of the paper is organized as follows. Section 2 introduces the system model and the main assumptions on system geometry, protocol settings, and client mobility. In Section 3, we propose a method for estimating the achievable data rate,

[4] QUALCOMM has already announced new 802.11ay chipsets, QCA6431 and QCA6421, intended for mobile use; however, the corresponding hardware specifications have not been published as of July 2019.

define the objective function, and formulate an optimization problem. Finally, Section 4 presents selected numerical results and main conclusions.

2 System model and assumptions

In this section, we introduce the main system assumptions on geometry and link abstraction, as well as describe the considered client mobility patterns.

2.1 System geometry and link abstraction

We consider a stationary IEEE 802.11ad/ay access point (AP), located at the origin A, and a dynamic device hereinafter termed client or user equipment (UE), which moves with the speed v in a selected direction (see Fig. 1). The UE mobility pattern is addressed below, and its initial location B is drawn from the uniform distribution in a circle of radius R around point A, where R defines the service area of the AP.

We assume that both devices can transmit directionally with the same antenna beam pattern, which is symmetrical w.r.t. the antenna boresight and characterized by the half power beam width (HPBW) θ. The resulting transmit/receive antenna gain may be approximated by the following function of the deviation α from the antenna boresight [16]:

$$G_{\text{tx/rx}} = D_0 \rho(\alpha), \tag{1}$$

where $D_0 = \frac{2}{1-\cos\frac{\theta}{2}}$ is the maximum antenna gain corresponding to $\alpha = 0$ and estimated as the ratio between the area of a sphere and the area of a cone antenna pattern, $\rho(\alpha)$ is the multiplier, which scales the antenna gain according to the deviation from the boresight, $\rho(\alpha) \in [0, 1]$ and $\rho(0) = 1$.

We note that $\rho(\alpha)$ and more precise value of D_0 can be estimated by using the data obtained in the course of measurement campaigns, in computational electromagnetics modeling tools, or via numerical evaluation of antenna arrays of a given structure, which is provided, e.g., by the corresponding MATLAB toolbox (that is, Sensor Array Analyzer). Here, we employ an approximation of the numerical function $\rho(\alpha)$ proposed in [16]. In particular,

$$\rho(\alpha) = \max\left(1 - \frac{\alpha}{\theta}, 0\right), \tag{2}$$

where θ is the HPBW and α is a current angular deviation of the transmit/receive direction from the antenna boresight. We let the AP (or UE) have M (N) predefined antenna beam patterns, i.e., for the AP, each m-th beam, $1 \le m \le M$, covers roughly a sector limited by angles in the interval $[2\pi\frac{m-1}{M}, 2\pi\frac{m}{M}]$. Then, we may assume HPBW of $\frac{2\pi}{M}$ and $\frac{2\pi}{N}$ for the AP and UE, correspondingly.

Further, we focus on the downlink transmission and assume that the line-of-sight connection between the devices exists at all times and, hence, the path loss can be estimated by the Friis equation. Consequently, we calculate the received power as

$$P_{\text{rx}} = P_{\text{tx}} G_{\text{tx}} G_{\text{rx}} \left(\frac{\lambda}{4\pi d}\right)^2, \tag{3}$$

where $G_{\mathrm{tx/rx}}$ are transmit/receive antenna gains, λ is the wavelength, d is the current distance between the transmitter (AP) and receiver (UE) located at points A and B, correspondingly.

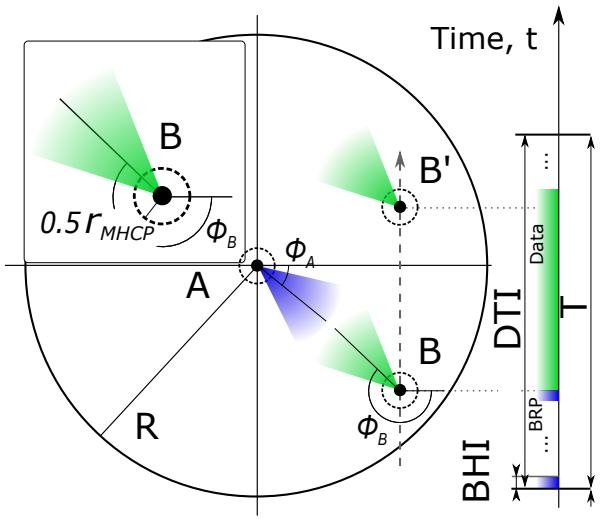

Fig. 1: Schematic illustration of the considered dynamic scenario: the client moves according to the rectilinear motion (gray dashed line) from point B to point B'. Initial beamforming (sector-level sweep for all UEs in the system) is performed during the time interval "BHI", and more refined alignment is achieved at the end of interval "BRP" (beam refinement protocol for this particular UE). After the data transmission "Data", the beam misalignment reaches the maximum, and the devices should initiate a new beamforming procedure.

2.2 Channel access abstraction

Beacon interval structure. If the UE moves on the plane while maintaining a highly-directional connection with the AP, the mutual alignment of the two antenna beams changes over time, and the devices need to update the beam directions by using, e.g., standard beamforming procedures. We assume that the time is divided into beacon intervals (BI) of length T that consist of (i) beacon header interval (BHI), where the devices perform initial beamforming (that is, sector-level sweep, SLS) and align their wider transmit beams, and (ii) the data transmission interval (DTI), incorporating service periods (SP) of different connected clients, while each SP contains beam refinement protocol (BRP) and the data transmission[5]. Fig. 1 schematically

[5] Here, we focus only on the scheduled operation, although DTI may as well contain contention-based access periods (CBAPs)

illustrates two phases, while Fig. 2 depicts a more detailed structure of the considered protocol. We note that since our system relies on highly-directional communication and implies the use of narrow beams, we may assume that after the beamforming procedure antenna beams are perfectly aligned.

If both devices were stationary, then after beamforming and during the data transmission of an arbitrary length, the antenna gains would reach its maximum. However, if either of the devices moves, then the received power and, hence, the achievable rate, may substantially drop due to the decrease in receive/transmit gain, which should be redressed at the next beamforming opportunity, e.g., in the following BI. The duration T of BIs (i.e., between the beginning of the adjacent BHIs) is an essential parameter affecting the overall performance of mmWave systems as, e.g., throughput, energy efficiency, data transmission delay, etc.

Sector-level sweep phase, SLS. At the beginning of each BI, in BHI, the AP performs SLS by sweeping through M_{SLS} transmit directions. We assume that the corresponding HPBW is given by $\theta_{\text{SLS,AP}} = \frac{2\pi}{M_{\text{SLS}}}$. Upon reception of the AP signal, the UE attempts to access the channel in the following interval (A-BFT, according to IEEE specifications) by selecting one of several time-divided transmission intervals, where the UE sweeps through N_{SLS} transmit beams with $\theta_{\text{SLS,UE}} = \frac{2\pi}{N_{\text{SLS}}}$. In A-BFT interval, if more than one clients select the same transmission opportunity, the signals collide, and devices cannot establish a connection in the current BI[6].

After SLS, both AP and UE know their best transmit beams, which are selected, in general case, based on the strongest received signal strength (RSSI). We remind that reception is (quasi-)omnidirectional at this phase[7].

The protocol limits the duration of the BHI, but we intentionally leave it flexible to investigate the corresponding system trade-offs. Hence, we assume that T_{SLS} can be derived according to the formula:

$$T_{\text{SLS}} = (M_{\text{SLS}} + n_a N_{\text{SLS}})\, \tau_{\text{SLS}}, \tag{4}$$

where τ_{SLS} is the duration of each sector sweep packet and n_a is the total number of transmission attempts in A-BFT. We assume that n_a is sufficiently large to minimize the channel collisions and neglect their effect in our model.

Beam refinement phase, BRP. After the SLS phase, the AP and the UE have established preliminary connection relying on relatively wide beams. The following service period (in DTI) allocated explicitly for the tagged UE, may start with beam refinement to improve the resulting instantaneous data rate.

[6] In fact, one of the clients may succeed. We leave the evaluation of initial random access collisions out of the scope of this paper. The detailed description of the protocol may be found in [17].

[7] In reality, the antenna pattern is not omnidirectional. Moreover, devices may use several directional antennas, and all of them participate in sector sweep. For the sake of clarity, we omit consideration of more complex procedures with multiple antennas but note that the respective modifications can be easily incorporated into our system.

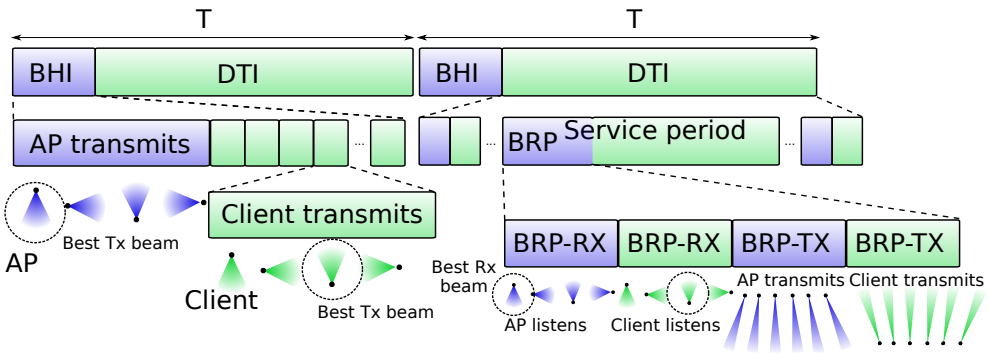

Fig. 2: Beacon interval structure.

Specifically, BRP may include both receive and transmit antenna training (as shown in Fig. 2) for the AP and the UE. We assume that the number of beams at this phase is defined by $M = bM_{\text{SLS}}$ ($N = bN_{\text{SLS}}$), where N_{SLS} is the number of the transmitter beams during SLS and $b > 1$ is a scaling multiplier, which we hereinafter term a beam refinement factor. Therefore, during the transmit antenna training, both devices sweep through exactly b narrower beams (within the initial transmit sector), while for receive training, all M or N directions should be covered. Thus, if we denote the duration of one BRP packet as τ_{BRP}, the total time spent on beam refinement is defined by

$$T_{\text{BRP}} = (2b + N + M)\,\tau_{\text{BRP}}. \tag{5}$$

Data transmission. The DTI may contain SPs scheduled during BHI or contention-based access periods (CBAPs). The use of CBAPs proved much less effective [18] and, therefore, in this work, we assume that only SPs are used for the data transmission. Moreover, we focus on one link, abstracting away the presence of other clients. Therefore, for simplicity, we assume that the scheduler follows round-robin policy, and our tagged client obtains and fully occupies, on average, $1/U$ of the total time resource, where U is the average number of clients per AP.

The duration of the time when devices are exchanging data traffic may be then found from the following equality:

$$T = T_{\text{SLS}} + U\,(T_{\text{BRP}} + T_{\text{DT}}) + T_0, \tag{6}$$

where T_{DT} is the duration of data transmission for one UE and T_0 is the total signaling overhead independent of the number of beams. We note that in (6), $T_{\text{SLS}} + UT_{\text{BRP}}$ depends on the beam settings, i.e., the number (and the width) of beams M, M_{BRP} and N, N_{BRP}, while T_{DT} is a variable that is to be properly selected to maximize the data rate as detailed in Section 3.

2.3 Mobility model

We assume that the receiver moves according to the random walk (RW) model and, hence, its path consists of a sequence of steps of length l taken in a random direction that is represented by angle γ (γ is calculated counterclockwise starting at the abscissa).

The length l can be expressed via the speed v of the moving client, i.e., $l = vT$, where T is a duration of one mobility step. Thus, the increments of coordinates

$$\Delta X_B = l \cdot \cos\gamma \quad \text{and} \quad \Delta Y_B = l \cdot \sin\gamma$$

determine new coordinates $(X_B + \Delta X_B, Y_B + \Delta Y_B)$ of the UE.

In our simulation setup, we guarantee the minimum distance between the receiver and the transmitter, introducing the minimum distance r_{MHCP} by analogy with Matern Hard Core Point process type-1 (MHCP-1) so that

$$d = \sqrt{(X_B - X_A)^2 + (Y_B - Y_A)^2} \geq r_{\text{MHCP}}.$$

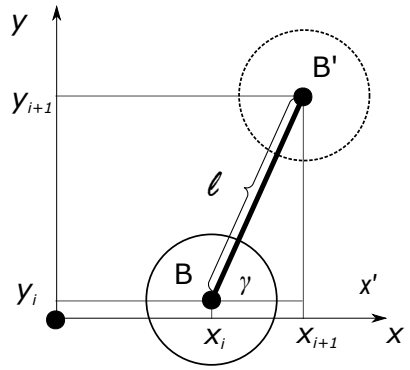

Fig. 3: Illustration of one step in the considered mobility models.

We consider three RW models: (i) rectilinear motion (no change in direction and, hence, in γ), (ii) random increment in direction γ that follows the normal distribution $N(0, \delta^2)$, and (iii) random walk on a grid, i.e., with the equiprobably distributed directions. Below we address these three models in detail.

Random walk model with the constant direction of motion. Uniform rectilinear motion is a special case of RW with the constant distance l and constant direction of motion $\gamma = \frac{\pi}{2}$ as illustrated in Fig. 1. In this case, increments of coordinates equal $\Delta X_B = 0$, $\Delta Y_B = l$.

Random walk with the normally distributed direction. Here, the distance l per cycle is constant, and the deviation of the direction of movement from the abscissa is a normally distributed random variable $\gamma \sim N(0, \delta^2)$. We assume that the standard

deviation δ is given by $\delta = \pi/2$ and, therefore, approximately 95% of γ fall into the interval $[-\pi, \pi]$.

Random walk on a grid. In this model, the distance l is constant, and the angle γ is a random variable, which at each step equiprobably accepts one of the following values: $\gamma \in \left\{0, \frac{\pi}{2}, \pi, \frac{3\pi}{2}\right\}$.

3 Optimization problem

In this section, we formulate an optimization problem that maximizes the achievable data rate for the given beamwidth and client mobility model.

As the data is transmitted only during the SP excluding BRP, i.e., during the time T_{DT}, the average achievable data rate is calculated by subtracting the corresponding overhead on SLS and BRP from the instantaneous rate. The instantaneous data rate is estimated by Shannon's limit constrained by the choice of modulation coding scheme (MCS), i.e.,

$$D = W \log_2 \left(1 + \min\left(\frac{P_{\mathrm{rx}}}{P_{\mathrm{noise}}}, \mathrm{SNR}_{\max}\right)\right), \tag{7}$$

where $\mathrm{SNR}_{\max}$ corresponds to the SNR value, at which the maximum MCS is selected, P_{rx} incorporates both transmit and receive antenna gains after the BRP phase (that is, w.r.t. the antenna beam misalignment, if any), $P_{\mathrm{noise}} = W \cdot N_0 \cdot \mathrm{NF}$, NF is the noise factor, and the interference is assumed to be negligible.

Consequently, if T_{DT} is significantly large, then during this time interval, the antenna alignment changes as the client moves forward and, hence, the instantaneous data rate gradually degrades. Alternatively, if the interval T_{DT} is short, and the configuration of the antenna beams does not noticeably change due to the client mobility, then the instantaneous data rate remains much higher; however, due to overhead $T_{\mathrm{SLS}} + UT_{\mathrm{BRP}}$, the actual average data rate during the BI decreases. This trade-off dictates the necessity of choosing an optimal value for the length T_{DT} (or, equivalently, T) that would maximize the average data rate, and results in an optimization problem below.

For our system with clients moving according to the RW model with the constant speed, the optimization problem can be formulated as

$$\begin{aligned} &D(T) \underset{T}{\rightarrow} \max \qquad \text{or, equivalently, find} \qquad T^* = \arg\max D(T) \\ &\text{subject to} \quad T > T_{\mathrm{SLS}} + UT_{BRP}. \end{aligned} \tag{8}$$

While the client moves, we measure the instantaneous data rate within the DTI at discrete time instants and average the rate over the actual duration of data transmission as

$$D_{\mathrm{DT}} = \frac{1}{J} \sum_{j=0}^{J} D_j, \tag{9}$$

where J is the number of time slots within one interval of data transmission. The resulting data rate per client is, therefore, defined by

$$D(T) = \frac{D_{\mathrm{DT}} T_{\mathrm{DT}}}{T}, \tag{10}$$

where the multiplier $\frac{T_{\mathrm{DT}}}{T}$ allows us to subtract the beamforming overhead and the time scheduled for other AP clients. The sought optimal BI duration T can be obtained numerically, which we demonstrate in the following section.

4 Numerical results and conclusions

Table 1: Simulation parameters.

Parameter	Value	Description
λ	0.005 m	Wavelength
f_c	60 GHz	Carrier frequency
R	40 m	Service area radius
P_{tx}	10 dBm	Transmit power
N_0	-174 dBm/Hz	Noise power per 1 Hz
NF	6 dB	Noise figure
W	2.16 GHz	Bandwidth
n_a	40	Number of slots in A-BFT
$\mathrm{SNR}_{\max}$	20 dB	SNR corresponding to choosing MCS19 (rate 13/16)
M	4, 8, 16	Number of AP transmit beams
N	4, 8, 16	Number of client transmit beams
τ_{SLS}	16 μs	Duration of one packet in SLS
τ_{BRP}	0.7 μs	Duration of one packet in BRP
v	var	Client speed

In this section, we present selected results of our numerical optimization. In general, we assume numerology of IEEE 802.11ay in its basic configuration (one channel, one spatial stream), the core simulation parameters are given in Table 1.

We begin with analyzing the dependence of the average data rate on the BI length for three considered mobility models and different values of the client speed (pedestrian 1.1 m/s, bicycle 5 m/s, and vehicle/drone 25 m/s). The rectilinear motion (movement along a straight line) is typical for cars on a highway or drones in the air. Another realistic pattern, with a pronounced drift, can be modeled by the normal distribution of the movement direction. Finally, RW on a grid may describe a chaotic movement of customers, for example, during a crowded large-scale open-air event. For the rectilinear motion, we set $\gamma = \pi/2$, while for the second mobility model $\gamma \sim N(0, \pi/2)$, and for the RW on a grid, γ is randomly and equiprobably selected, $\gamma \in \{0, \pi/2, \pi, 3\pi/2\}$.

As shown in Fig. 4, in the case of the rectilinear motion and mobility with normally distributed directions at high speed ($v = 25$ m/s), the data rate starts decreasing already after approximately 100 ms, while for the lower speeds, $v = 1.1$ m/s and 5 m/s, the optimal BI interval length increases up to 500 ms and 250 ms, respectively. In all cases, the rate curves rise abruptly at the beginning of the abscissa (where T remains small), since the overhead occupies noticeably long time w.r.t. the total BI duration. When the time allocated for the data transmission increases, the data

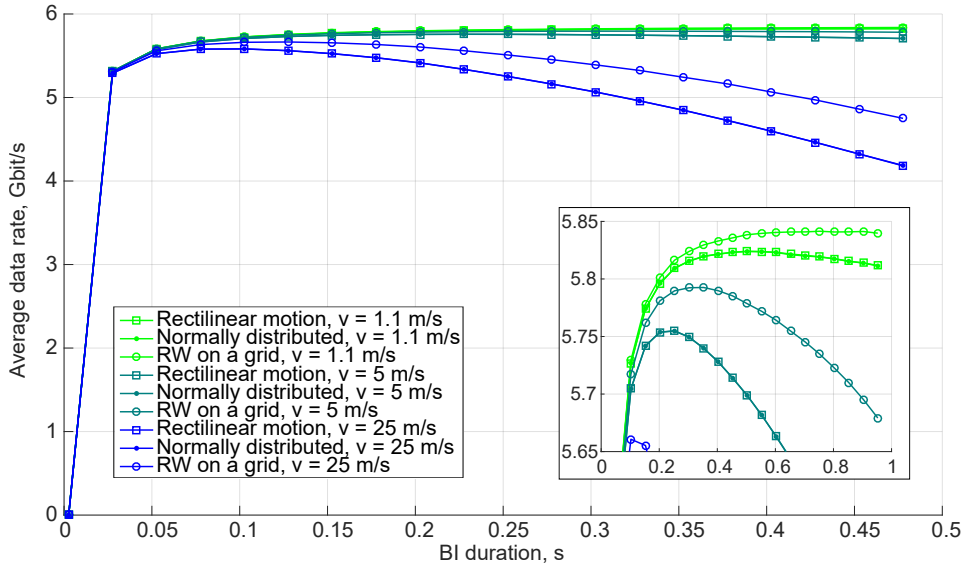

Fig. 4: The average data rate vs. the BI length for different mobility patterns and speeds. The HPBW $\theta = 45°$.

rate quickly reaches the maximum and then declines much slower due to the beam misalignment.

Moreover, for the rectilinear motion and mobility pattern with normally distributed directions, the data rate decreases visibly faster than in the case of the RW on a grid. This effect may be explained by the fact that clients moving on a grid stay within the same region longer than if they rapidly moved away along a concrete direction.

Further, we continue by varying the beamwidth, $\theta = 11°, 22°, 45°$ (see Fig. 5). For the lower speeds, the narrower beams guarantee better data rate due to higher antenna gains; however, for the higher speeds, there exists a trade-off between the increasing gains and even faster beam misalignment of narrow beams (see the group of curves for $\theta = 11°$ that). In general, the optimal BI duration becomes longer if we decrease θ due to the large overhead. Importantly, even for these settings, our system continues to function well since we assume 802.11ay BRP timings that are much more effective than those of 802.11ad.

Finally, in Fig. 6, we provide an important practical trade-off that may help in selecting optimal BI duration in scenarios with different client mobility. Naturally, when the speed grows, the optimal BI duration decreases and for narrower beams remains larger in most cases (as confirmed by results in Fig. 6). However, at the lower speeds ($0 - 5\,\mathrm{m/s}$), the optimal BI for $\theta = 22°$ due to the high antenna gain is significantly longer than that of for $\theta = 11°$. As the speed grows, the difference between the optimal BI values for narrow and wider beams is diminished and may

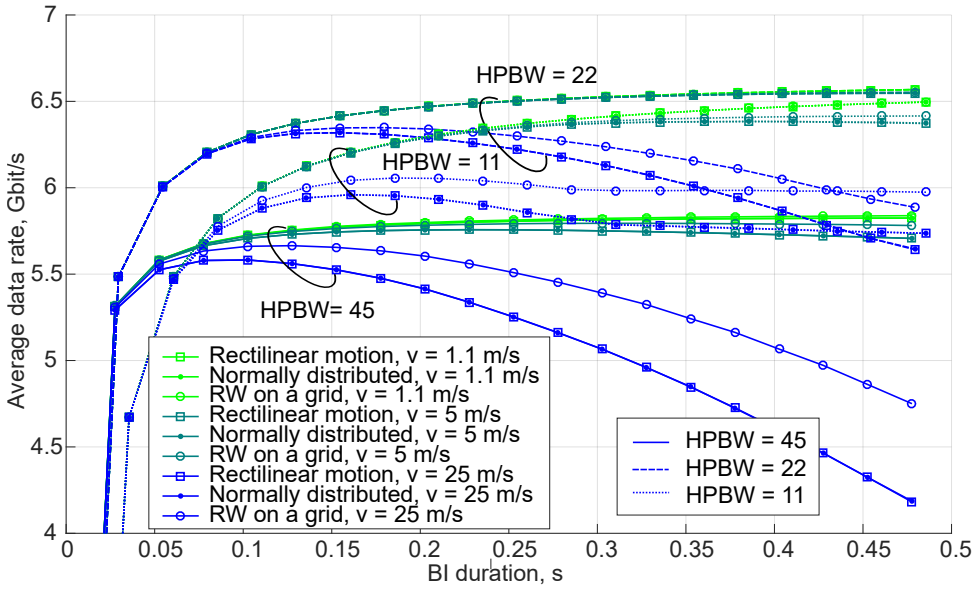

Fig. 5: The average data rate for different HPBW ($\theta = 11°, 22°, 45°$).

fluctuate around approximately the same value of the BI duration, which should be further investigated in more details.

In summary, we may conclude that in order to determine the optimal BI duration in highly mobile scenarios, it is necessary to take into account a combination of multiple factors, such as mobility pattern, client's speed, and the structure of the wireless protocol. A promising future direction could be found, e.g., in defining practically feasible (or even adaptive) heuristics through analytical optimization of a simplified system, more detailed analysis of periodicity of BRPs within one SP, effects of heterogeneous time and space data demand, and mobility of blockers and APs.

References

1. N. Jones, "The top 10 wireless technologies and trends that will drive innovation," 2019.
2. Y. Ghasempour, C. R. da Silva, C. Cordeiro, and E. W. Knightly, "Ieee 802.11 ay: Next-generation 60 ghz communication for 100 gb/s wi-fi," *IEEE Communications Magazine*, vol. 55, no. 12, pp. 186–192, 2017.
3. IEEE 802.11 Working Group, "IEEE 802.11 TGay Use Cases," 2015.
4. C. Cordeiro, D. Akhmetov, and M. Park, "Ieee 802.11 ad: Introduction and performance evaluation of the first multi-gbps wifi technology," in *Proceedings of the 2010 ACM international workshop on mmWave communications: from circuits to networks*, pp. 3–8, ACM, 2010.

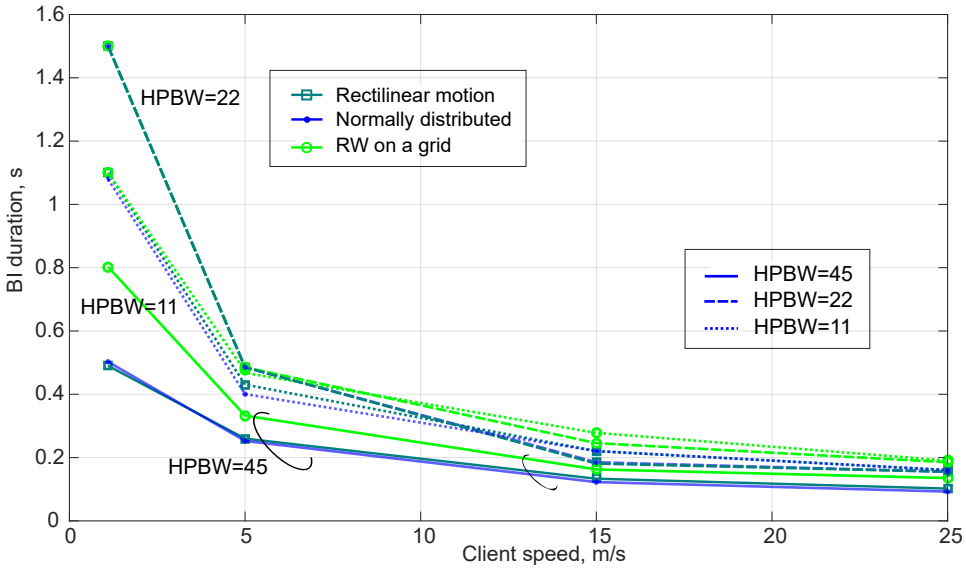

Fig. 6: The optimal BI vs. the client speed for three mobility models.

5. J. Kim and A. F. Molisch, "Enabling gigabit services for ieee 802.11 ad-capable high-speed train networks," in *2013 IEEE Radio and Wireless Symposium*, pp. 145–147, IEEE, 2013.
6. L. Verma, M. Fakharzadeh, and S. Choi, "Wifi on steroids: 802.11 ac and 802.11 ad," *IEEE Wireless Communications*, vol. 20, no. 6, pp. 30–35, 2013.
7. T. Nitsche, C. Cordeiro, A. B Flores, E. W. Knightly, E. Perahia, and J. Widmer, "IEEE 802.11ad: directional 60 GHz communication for multi-Gigabit-per-second Wi-Fi," *IEEE Communications Magazine*, vol. 52, no. 12, pp. 132–141, 2014.
8. K. Zeman, M. Stusek, J. Pokorny, P. Masek, J. Hosek, S. Andreev, P. Dvorak, and R. Josth, "Emerging 5g applications over mmwave: Hands-on assessment of wigig radios," in *2017 40th International Conference on Telecommunications and Signal Processing (TSP)*, pp. 86–90, IEEE, 2017.
9. C. R. Da Silva, J. Kosloff, C. Chen, A. Lomayev, and C. Cordeiro, "Beamforming training for IEEE 802.11ay millimeter wave systems," in *2018 Information Theory and Applications Workshop (ITA)*, pp. 1–9, IEEE, 2018.
10. C. R. da Silva, A. Lomayev, C. Chen, and C. Cordeiro, "Analysis and simulation of the ieee 802.11 ay single-carrier phy," in *2018 IEEE International Conference on Communications (ICC)*, pp. 1–6, IEEE, 2018.
11. V. Va, T. Shimizu, G. Bansal, and R. W. Heath, "Online learning for position-aided millimeter wave beam training," *IEEE Access*, vol. 7, pp. 30507–30526, 2019.
12. P. Kumari, M. E. Eltayeb, and R. W. Heath, "Sparsity-aware adaptive beamforming design for ieee 802.11 ad-based joint communication-radar," in *2018 IEEE Radar Conference (RadarConf18)*, pp. 0923–0928, IEEE, 2018.
13. V. Va, J. Choi, T. Shimizu, G. Bansal, and R. W. Heath, "Inverse multipath fingerprinting for millimeter wave v2i beam alignment," *IEEE Transactions on Vehicular Technology*, vol. 67, no. 5, pp. 4042–4058, 2018.

14. A. Samuylov, M. Gapeyenko, D. Moltchanov, M. Gerasimenko, S. Singh, N. Himayat, S. Andreev, and Y. Koucheryavy, "Characterizing spatial correlation of blockage statistics in urban mmwave systems," in *2016 IEEE Globecom Workshops (GC Wkshps)*, pp. 1–7, IEEE, 2016.
15. M. Gapeyenko, A. Samuylov, M. Gerasimenko, D. Moltchanov, S. Singh, M. R. Akdeniz, E. Aryafar, N. Himayat, S. Andreev, and Y. Koucheryavy, "On the temporal effects of mobile blockers in urban millimeter-wave cellular scenarios," *IEEE Transactions on Vehicular Technology*, vol. 66, no. 11, pp. 10124–10138, 2017.
16. O. Chukhno, N. Chukhno, O. Galinina, Y. Gaidamaka, S. Andreev, and K. Samouylov, "Analyzing effects of directional deafness on mmwave channel access in unlicensed bands," in *accepted to IEEE GLOBECOM 2019*, 2019.
17. IEEE 802.11 Working Group, "Wireless LAN Medium Access Control (MAC) and Physical Layer (PHY) Specifications. Amendment 3: Enhancements for Very High Throughput in the 60 GHz Band," 2012.
18. O. Galinina, A. Pyattaev, K. Johnsson, A. Turlikov, S. Andreev, and Y. Koucheryavy, "Assessing system-level energy efficiency of mmwave-based wearable networks," *IEEE Journal on Selected Areas in Communications*, vol. 34, no. 4, pp. 923–937, 2016.